15

Effect of Spark Plasma Sintering in Fabricating Carbon Nanotube Reinforced Aluminum Matrix Composite Materials

Hansang Kwon[1] and Akira Kawasaki[2]
[1]*Advanced Materials Processing, Empa-Swiss Federal Laboratoriesfor Materials Science and Technology, Thun,*
[2]*Department of Materials Processing, Tohoku University, Sendai,*
[1]*Switzerland*
[2]*Japan*

1. Intorduction

Carbon nanotubes (CNT) are attractive next generation materials due to their unique properties, which lead to high mechanical, electrical, and thermal performance (Iijima, 1991; Endo et al., 1976; Niyogi et al., 2002; Komarov & Mirnov, 2004). This unique nano order material can not only be utilized on its own in precision industrial fields but can also provide high performance functionality in conjunction with conventional materials. For this reason, many researchers are investigating the fabrication of CNT reinforced metal, ceramic, and polymer matrix composite materials. Despite their research efforts, the fabrication of CNT-reinforced metal matrix composite materials, particularly with an aluminum (Al) matrix, is still facing several problems, such as difficulties in homogeneously dispersing the CNT in the Al matrix, (Salvetat-Delmotte and Rubio, 2002; Hilding et al., 2003; Xu et al., 1999) producing highly densified composite materials without any degradation of the CNT, (Kuzumaki et al., 1998; Sridhar & Narayana, 2009) and achieving enough interface strength between the Al matrix and reinforcement of CNT (Deng et al., 2007; Bakshi et al., 2009; Lahiri et al., 2009). To overcome these problems, Deng et al. fabricated the CNT-Al alloy composite materials by cold isostatic pressing and then subsequent hot extrusion techniques, with which they have achieved 45% incremental increase in tensile strength (Deng et al., 2007) Esawi et al. attempted to fabricate a CNT-Al matrix composite by mechanical milling and rolling or extrusion processes (Esawi & Morsi, 2007; Esawi & Borady, 2008; Esawi et al., 2009). Morsi et al. produced CNT-Al matrix composites by a unique powder metallurgy route using spark plasma extrusion (Morsi et al., 2009; 2010). Agawal et al. introduced several fabrication methods for CNT-Al and Al alloy composites based on thermal and cold spray forming technologies (Laha et al., 2004; Bakshi et al., 2008; Bakshi & Agarwal, 2010). Recently, we have also demonstrated the feasibility of making aluminum-carbon nanotube (Al-CNT) composite materials, producing not only a highly densified composite but also enhanced interface bonding between the Al matrix and CNT, by a combination of spark plasma sintering (SPS) followed by hot extrusion processes (Kwon et al., 2009; Kwon & Kawasaki, 2009; Kwon et al., 2010). However, the specific effect

of SPS for the final product of Al-CNT composite is not yet clear. In the present study, we have fabricated CNT reinforced aluminum matrix composite materials with two different amounts of CNTs (1 and 5vol%), by a combination of SPS followed by hot extrusion processes. Pure Al bulks also have been fabricated using the same route for comparison. In particular, the SPS behavior of the Al-CNT mixture powder was discussed. Firstly, the morphologies of Al grains in spark plasma sintered (SPSed) Al-CNT and pure Al compacts were observed. The chemical stability between the Al and CNT and the real temperature between the each Al particles during the SPS process were discussed based on the two particles model. Finally, high resolution transmission electron microscopy was carried out to understand the materials at the boundary of the SPSed Al-CNT compact. Moreover, the tensile strength and elongation of the composites was measured and discussed in relation to the different amounts of CNT additions.

2. Experimental procedure

A precursor aimed at dispersing CNTs well was produced by the nanoscale dispersion method (Kwon et al., 2009; Noguchi et al., 2004). The precursor consisted of commercial gas atomized Al powder (ECKA Granules Co. Ltd., Japan, purity 99.85%, average particle size 14.82μm), multi-walled carbon nanotube (MWCNT, ILJIN Co. Ltd., Korea, purity 99.5%, average diameter and length 20 nm and 15μm), and natural rubber (NR). The powder composition was adjusted to 1 and 5vol% of CNT. The CNT was mixed with NR in benzene and then Al powder was added. This Al-CNT-NR (precursor) was roll-milled to a thickness of 2 mm and a sheet shape was formed. A thermal gravimetric analysis (TGA6300, SEIKO Instruments, Inc., Japan) was carried out to check the specific decomposition temperature of the NR in argon atmosphere from the precursor. The heating and flow rate were fixed at 10 °C/min and 50 m*l*/min, respectively. The precursor was heat-treated in a quartz tube furnace (Shimadzu Co. Ltd., Japan) at 500 °C for 2h under an argon atmosphere with a 1*l*/min flow rate to evaporate the NR. The obtained Al-CNT mixture powder was sintered at 600 °C, with a holding time of 20 min, a heating rate of 40 °C/min, and a pressure of 50MPa in a ϕ15 mm carbon mold, using a SPS device (SPS-S515) manufactured by Sumitomo Coal Mining Co. Ltd, Japan. The sintered compact was extruded in a 60° conical die at 400 °C with a 500kN press (UH-500kN1, Shimadzu Corporation, Japan). The extrusion velocity and extrusion ratio were fixed at 2mm/min and 20, respectively. The microstructures of the samples after each step were observed by optical microscopy (PMG-3, OLYMPUS, Japan), field-emission scanning electron microscopy (FE-SEM) (FE-SEM6500, JEOL Ltd, Japan) and high-resolution transmission electron microscopy (HR-TEM) (HITACHI 200, Japan) with energy dispersive spectrometry (EDS, 5 nm spot size) and selected area diffraction pattern (SADP, under 10 nm nano-beam spot size and 1.2 m camera lens distance from specimen). Raman spectroscopy (SOLAR TII Nanofinder, Tokyo Instruments Co. Ltd, Japan) was employed to evaluate the disorder ratio of the CNTs after each step. The chemical stability between the CNT and Al powder was analyzed using a differential scanning calorimeter (DSC6300, SEIKO Instruments, Inc., Japan) in a purified argon atmosphere at 800 °C and a scanning rate of 10 °C/min. To evaluate the tensile strength, the extruded composites were machined into test pieces 3 mm in diameter, in accordance with ICS 59.100.01. The tensile strength was measured with a universal testing machine (AUTOGRAPH AG-I 50 kN, Shimadzu Co. Ltd, Japan)

3. Results and discussion

Figure 1 shows FE-SEM and TEM micrographs of the raw Al and CNT as-received powders. The Al particles show several size distributions and a spherical shape, as shown in Figure 1a. The morphology of the raw CNT has an extremely zigzagged shape with a high aspect ratio, as shown in Figure 1b. The out-wall of the CNT consisted of some disordered regions and amorphous carbon as shown by the black arrow in Figure 1c. Two different tip shapes of CNT were observed, opened and closed as shown by the white arrows in Figure 1c. It was found that the I_D/I_G (intensity ration of graphite and defect peaks in the CNT) ratio of the raw CNT observed from the Raman spectra (Keszler et al., 2004; Zhao & Wagner, 2004) was about 0.8, which means a relatively high number of defects and contaminants, as indicated in Table 1.

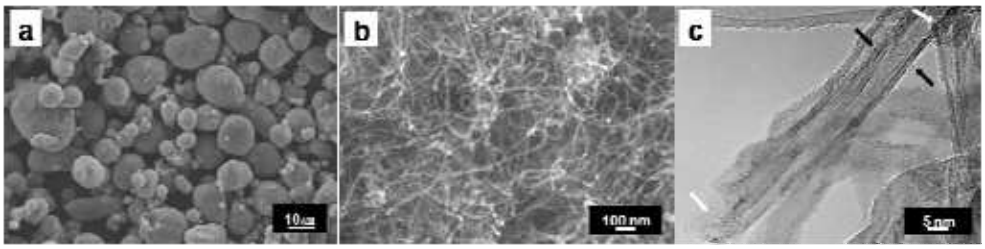

Fig. 1. FE-SEM micrographs of (a) as-received Al powders and (b) CNT. (c) HR-TEM micrograph of the pristine CNT. The white and black arrows indicate some disordered and amorphous impurity.

	Relative density (%)	I_D/I_G ratio (±10%)	Boundary thickness (nm)	Tensile strength (MPa ±10%)	Elongation (% ± 10%)
Heat treated Al-CNT powder	-	Raw CNT:0.877 Al-CNT:0.831	-	-	-
SPSed Al-1vol.% CNT compact	96.3	072	~100	-	-
SPSed Al-5vol.% CNT compact	96.1	0.85	~300		
Extruded Al-1vol.% CNT composite	98.6	0.79	~60	198.8	21.9
Extruded Al-5vol.% CNT composite	98.0	0.843	~200	187.3	10.5
Extruded pure Al bulk	100	-	15	52	19.5

Table 1. Various properties of SPSed Al-CNT compact and extruded Al bulk and Al-CNT composites.

TGA measurement was carried out to confirm the specific decomposition temperature for NR in the Al-CNT-NR mixture, as shown in Figure 2. A slight weight loss was observed for the mixture in the region of around 200 °C, which may be due to the removal of some organic contaminants and adsorbed moisture. A dramatic weight loss of about 15% was detected between 350-450 °C, which was due to the complete removal of NR. This demonstrated that the NR as a mixing medium could be completely removed from the Al-NR-CNT mixture at less than 450 °C. Based on the TGA result, we carried out a heat treatment for the precursor at 500 °C for 2 h.

Figure 3 shows FE-SEM micrographs of the Al-CNT mixture powders after removal of NR from the Al-CNT-NR precursor. The Al particles maintained their initial spherical morphology and particle size after heat treatment, as per those of the starting powder, as

shown in Figure 2a and 3a (1vol%) and b (5vol%). Some regions with agglomerated CNTs were observed after the removal of NR from the Al-NR-CNT precursor, which may be due

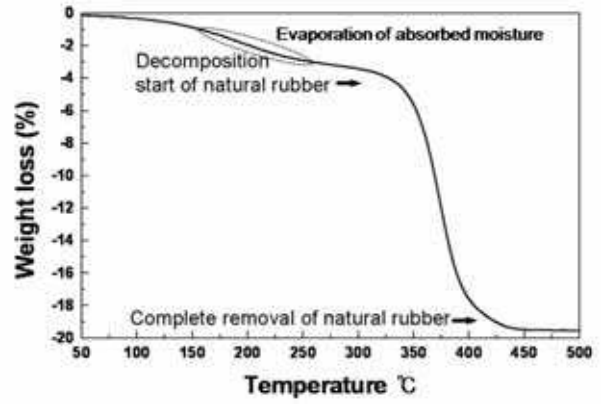

Fig. 2. TGA curve of Al-NR-CNT precursor.

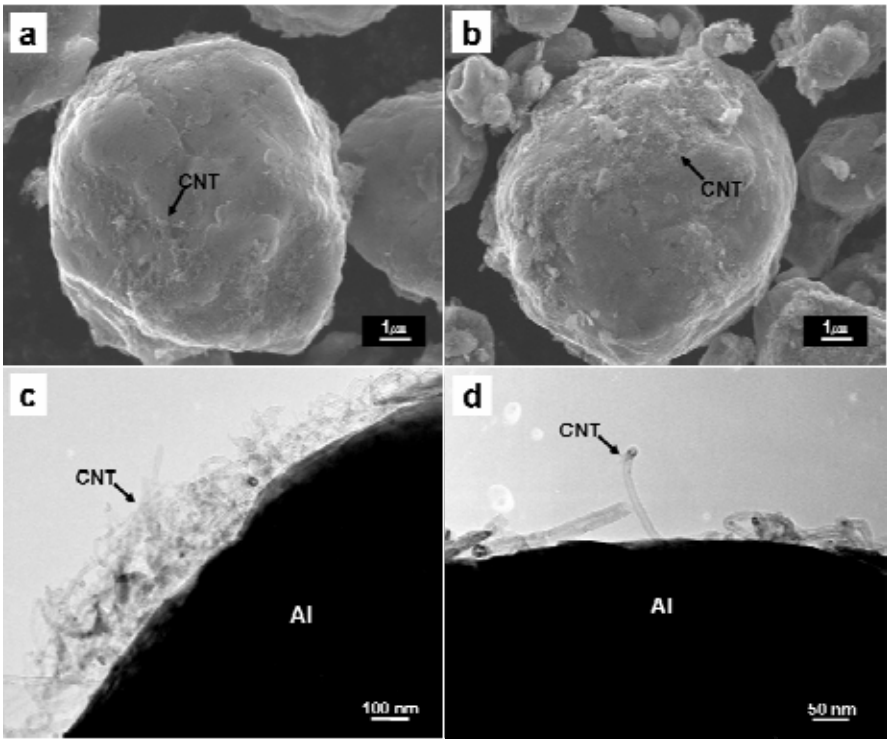

Fig. 3. FE-SEM micrographs of (a) Al-1vol% CNT and (b) Al-5vol% CNT mixture powders. HR-TEM micrographs of (c) condensation and (d) dispersed region of CNT on the Al particle in the Al-5vol% CNT mixture powder.

to the selective condensation of CNTs located where the NR was removed from between Al particles**.** Moreover, this CNT agglomerate ratio was relatively higher in the 5vol% CNT mixture powder than in the Al-1vol% CNT mixture powder, as shown in Figure 3a and b. We believe that this problem can be addressed by adjusting the Al particle size distribution. Overall, our findings indicated that most of the CNTs were well dispersed on the surface of Al particle, regardless of the amount of CNT added.

The relative density of pure Al bulk and Al-1 and 5vol% CNT composites subjected to the same processes were measured by an Archimedes method (Table 1). It was found that the extruded pure Al bulk was fully densified and the SPSed Al-CNT compact and extrudate were also highly densified, demonstrating that this combination of SPS and hot-extrusion processes is highly effective in densifying the Al-CNT mixture powder.

The tensile strength and elongations of the pure Al bulk and the composites are indicated in Table 1. The composites showed around 300% enhancement in tensile strength compared to that of the pure Al bulk. In particular, no degradation of elongation for the Al-1vol% CNT composite was observed, in spite of the highly enhanced tensile strength. In general, the nominal tensile strength of pure Al (http://en.wikipedia.org/wiki/Tensile_strength) was reported as about 40-50 MPa whereas the tensile strength of the extruded pure Al bulk obtained in this study was 52 MPa (Table 1). This small disagreement originated from differences in fabrication and testing conditions.

We have considered the effect of work hardening on tensile strength due to large plastic deformation in the processes employed. According to our previous report that used nano-indentation for work hardening, there was no change in the hardness of Al particles before and after the extrusion process (Kwon et al., 2009). It is suggested that the stress accumulation was lower than stress released during the extrusion process by dynamic recrystallization (Knocks, 2004; Kelly & Tyson, 1965; Cox, 1952; Serajzadeh, 2004). Therefore, the enhanced tensile strength of the composites with a small amount of CNT (1 and 5 vol%) is mainly due to the addition of CNT itself.

The tensile and elongation behavior should be considered with regard to the amount of CNT. It is assumed that the thickness of the dispersed CNT on the Al particle will be different depending on the amount of CNT added. i.e. the thickness of this CNT cluster could affect the mechanical properties of the composites, resulting in a large difference in elongation, as indicated in Table 1.

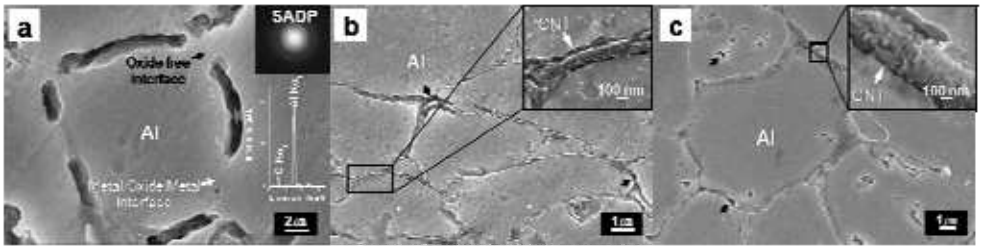

Fig. 4. FE-SEM micrographs of (a) the SPSed pure Al compact; the insets indicate the SADP and EDS of the boundary region (Kwon et al., 2010) (b) the SPSed Al-1vol% CNT compact, and (c) SPSed Al-5vol% CNT compact; the insets in (b) and (c) show a high magnification of the boundary region between Al and CNT.

Microstructures of the SPSed pure Al and Al-CNT compacts were observed in order to clarify the boundary structure. Firstly, the SPSed pure Al compact was investigated, as shown in Figure 4a. Several boundary grooves were observed after the etching process, which made use of liquid etchant (5 % NaOH). Thin layers (10-20 nm) of amorphous Al oxide and some oxide-free region (black arrow in Fig. 4a) in the boundary zone were observed by SADP and EDS, as shown in Figure 4a. Some of the Al oxide-free region was created by decomposition of Al oxide during the SPS process by micro-plasma (Zadra et al., 2007; Omori, 2000; Xie et al., 2001; Kwon et al., 2010). In the case of the SPSed Al-CNT compacts, the boundary structure was completely different to that of the pure Al compact. We observed boundary layers of around 100 and 300 nm thick for the 1 and 5 vol% CNT added compacts, respectively, as shown in Figure 4b and c. Several micro-pores were also observed regardless of the different amounts of CNT addition (black arrows in Fig. 4b and c). These pores may also include those produced during the etching process. Moreover, no significant grain growth was observed for both SPSed pure Al and Al-CNT compacts compared to the starting Al particles (see Fig. 1a and Fig. 4). We believe that the grain growth was restrained by the pinning effect of the CNTs, some of the existing Al oxide being present at the boundaries, and the quick processing cycle of SPS. Our previous results showed that the boundary of the SPSed Al-1 and 5vol% CNT compact contained mainly CNT, a small quantity of Al carbide (Al_4C_3), carbon black, amorphous carbon, Al oxide, and Al, which was confirmed by SADP and EDS as shown in Figure 5. (Kwon et al., 2009) The formation of Al_4C_3 in spite of being under the Al melting point will be discussed in depth later. However, it is understood that the thickness of the boundary (mainly CNT) can be changed by the amount of CNT addition.

Figure 6 shows TEM micrographs of the extruded Al-1 and 5vol% CNT composites. The thickness of the boundaries was slightly reduced after the extrusion process for Al-1 and 5vol% CNT composites to ~60 and ~200 nm, respectively, compared to that of the SPSed compacts, as indicated in Table 1. This slightly changed boundary thickness accompanied the large plastic deformation during the extrusion process. Furthermore, the CNT in the boundary were aligned with the extrusion direction and in tight contact with the Al matrix, as shown in Figure 6a and b. Hence, the applied pressure of extrusion affected not only the alignment of the CNTs but also the thickness of the boundary structure, regardless of the amount of CNT added. The implanted Al_4C_3 between the Al matrix and the CNT interface was observed in the 5vol% CNT composite, as shown in Figure 6c (Kwon et al., 2009). Such a microstructure also contributed to the enhancement of the mechanical properties of the composites. Figure 7 shows HR-TEM of the Al-1vol% CNT composite subjected to the extrusion process.

As can be seen in Fig. 7, two different types of aluminum carbide (Al_4C_3) were observed in the boundary zone, dumbbell and tube types (Kwon et al., 2010). We believe that dumbbell-shaped Al_4C_3 originated from the tip of a CNT, whereas tube-shaped Al_4C_3 originated from defective CNTs.

Here, we have discussed how the formation of Al_4C_3 was able to occur under the Al melting point. Figure 8 shows the DSC curves of the pure Al powder, Al-5vol% CNT powder, and SPSed (at 600 ^oC) Al-5vol% CNT compact. In the case of the powders, they showed endothermic peaks near the Al melting point (about 660 ^oC), as shown in Figure 8a and b. However, the SPSed Al-CNT compact showed an endothermic peak followed by an exothermic peak, as shown in Figure 8c. It indicated that a chemical reaction occurred,

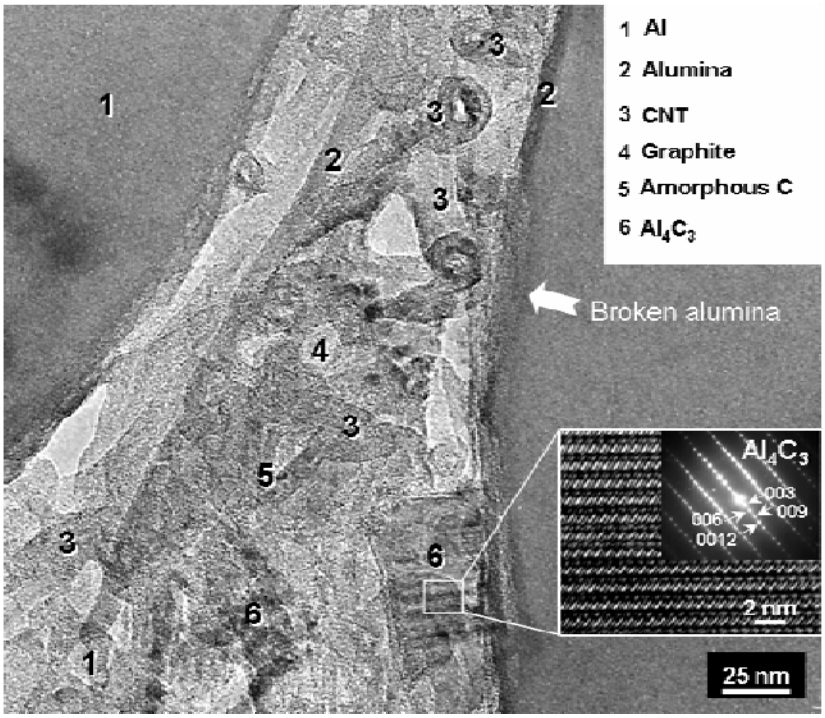

Fig. 5. TEM micrographs of the boundary layer of the SPSed Al-5vol% CNT compact. The boundary layer between the Al particles (1) consisting of alumina (2), CNT (3), amorphous carbon black (4), graphite (5), and Al_4C_3 (6) phases. The white arrow indicates broken alumina. The inset shows the SADP and HR-TEM micrographs of the Al_4C_3 phase (Kwon et al., 2009)

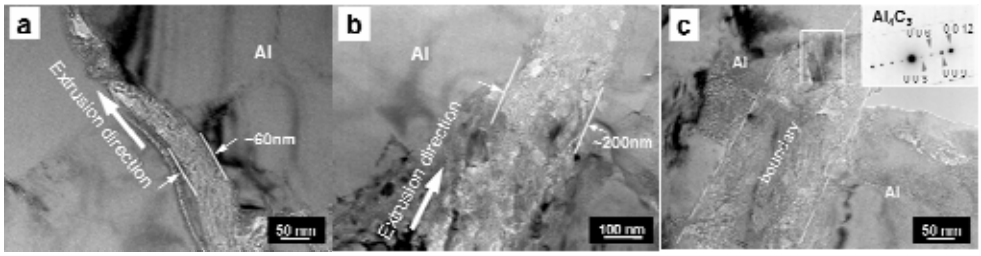

Fig. 6. TEM micrographs of (a) the extruded Al-1vol% CNT composite and (b) the extruded Al-5vol% CNT composite. (c) The implanted Al_4C_3 between the Al matrix and CNT in the Al-5vol% CNT composite (Kwon et al., 2009). The inset shows the SADP of the Al_4C_3.

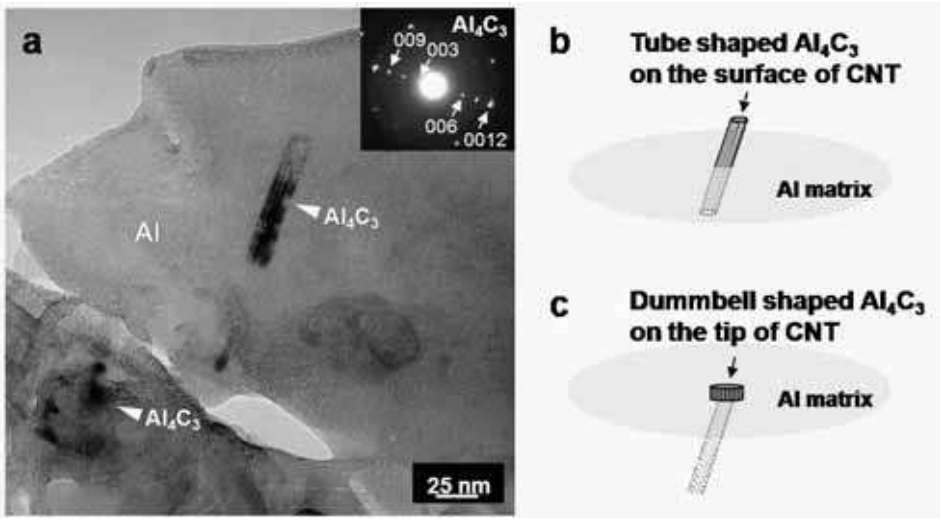

Fig. 7. HR-TEM images of the microstructure of Al–1vol% CNT subjected to the extrusion process. (a) The formation of Al_4C_3 was observed near the boundary zone. The inset confirms the crystal structure of Al_4C_3 by its selected-area diffraction (SAD) pattern. (b), (c) Tube-shaped Al_4C_3 was generated on the surface of defective CNTs, whereas particle-shaped Al_4C_3 was generated on the tips of CNTs. Both forms (b) and (c) were implanted into the Al matrix (Kwon et al., 2010).

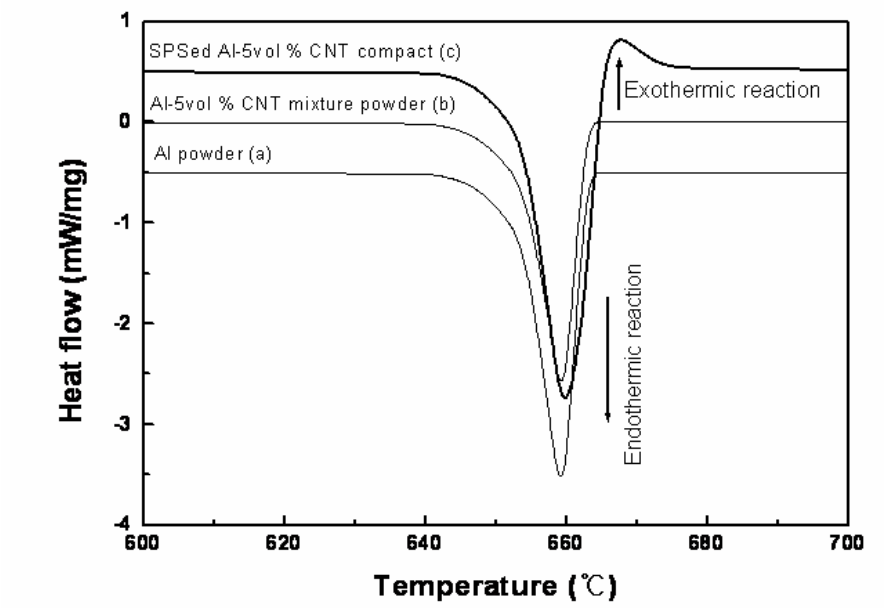

Fig. 8. DSC curves of the pure Al powder, Al-5vol% CNT powder, and 600 °C SPSed Al-5vol% CNT compact.

creating the exothermic peak right after the endothermic reaction**.** In general, it is known that the pure Al particle has a stable oxide layer on the surface of the particles (Zadra et al., 2007; Omori, 2000; Kwon et al., 2010). Therefore, the liquid Al generated is not able to flow out due to the presence of the Al oxide layer (melting point: <2000 °C) on the surface of the Al particle, even though the pure Al particle is completely melted. as illustrated by Figure 9a. For this reason, the Al-CNT mixture powder demonstrates the same phenomenon as in the case of the pure Al powder (Fig. 9b).

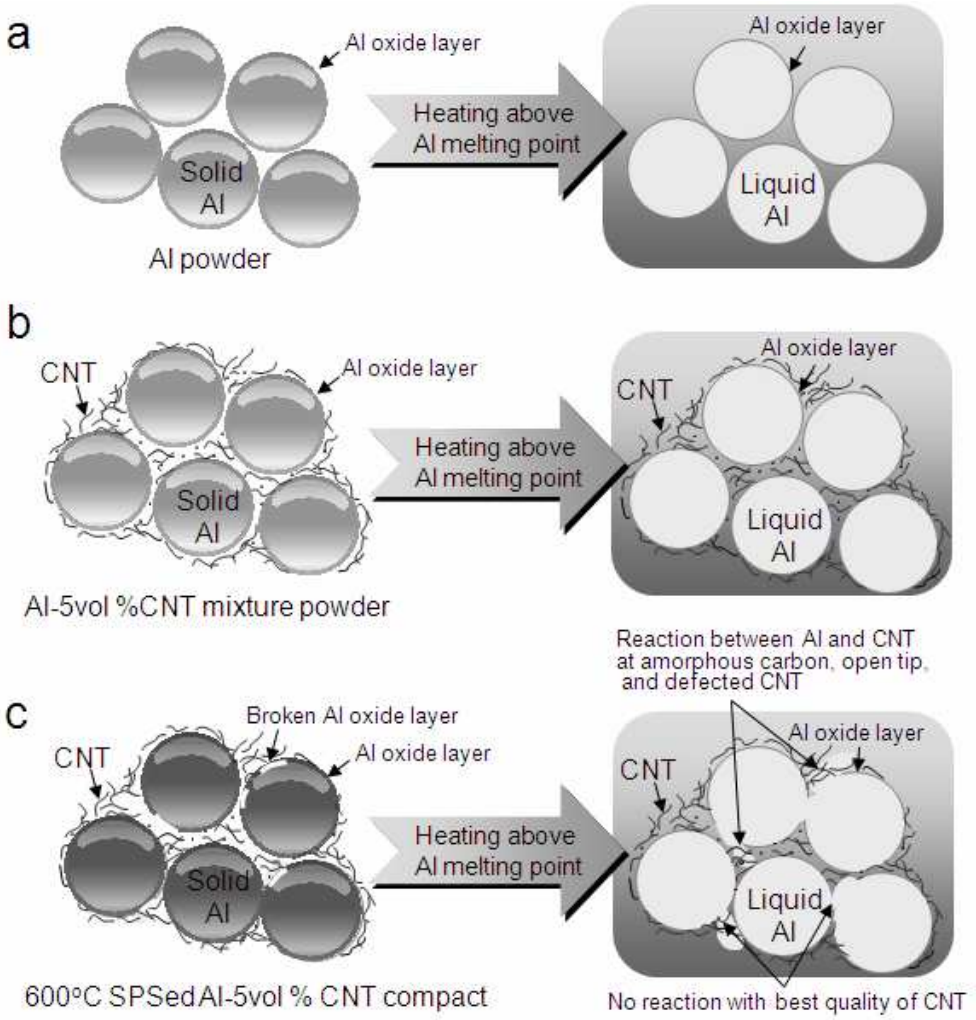

Fig. 9. Chemical stability of the CNT in the Al powder: (a) in the case of the pure Al powder, (b) Al-5vol% CNT mixture powder, and (c) 600 °C SPSed Al-5vol% CNT compact.

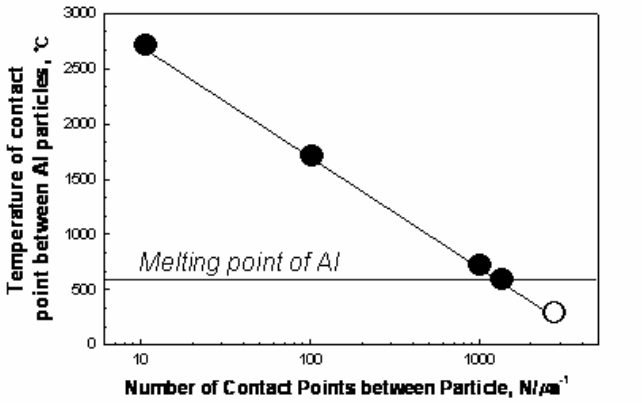

Fig. 10. Calculated temperature depends on the number of contact points between Al particles during the SPS process.

However, in the case of the SPSed Al-CNT compact, a different phenomenon is expected, because the SPSed Al-CNT compact possesses several broken parts of Al oxide layer induced during the SPS process by micro-plasma (Omori, 2000; Kwon et al., 2010). In this case, the liquid Al phase is able to flow out through several broken parts of the Al oxide layer, thereby making contact with the CNTs in the boundary layer when the SPSed Al-CNT compact is heated above the Al melting point, as shown in Figure 9c. In general, there is no chemical reaction between the Al liquid phase and CNTs with best-quality CNTs (which have no defects) (Ci et al., 2006). But disordered CNT, the amorphous carbon surface of the CNT, and opened-tips of the CNT lead to reaction with the Al liquid phase (Kwon et al., 2009; Ci et al., 2006; Laha & Argawal, 2008). According to the I_D/I_G ratio and TEM observation result of the raw CNT, it contained many structural defects, amorphous carbon, and opened-tip CNTs, as shown in Table 1 and Figure 1c, indicating that the CNTs used in the present work were highly likely to react with the Al liquid phase. Therefore, the exothermic peak that followed immediately after the endothermic peak can be attributed to the chemical reaction occurred between the Al and CNT, resulting in the formation of Al_4C_3 that was observed in the SPSed compact, as shown in Figure 5.

Nagae et al. reported the feasibility of generating an Al liquid phase under the Al melting point during the SPS process using a two-particle model based on the real temperature between the Al particles during the SPS process (Nagae et al., 2001). According to their calculations, the real temperature of the initial stage of sintering between the Al particles was about 1270 °C at the initial stage of the SPS process which is supposed to proceed at 570 °C. Figure 10 shows the calculated real temperatures between the Al particles using the two-particle model based on the SPS temperature of 600 °C used in the present study. The real temperature between Al particles decreased due to the increase in contact points as time passed. Thus, we believe that the real temperature between Al particles in the initial stage of the SPS process was higher than the sintering temperature employed. For this reason, the Al liquid phase can be generated at the SPS temperature employed in the present study, thereby creating the possible conditions for the formation of Al_4C_3.

The I_D/I_G ratio of the 5vol% CNT composite was higher than that for the 1vol% CNT composite (Table 1), resulting in the predominant formation of Al_4C_3 in the 5vol% CNT

composite. The 5vol% CNT composite showed a slightly lower tensile strength and much lower elongation than the 1vol% CNT composite, which may be due to the excessive Al_4C_3 generated, as indicated in Table 1. However, a moderate amount of Al_4C_3 can contribute to better chemical bonding between the Al matrix and CNT but too large an excess of Al_4C_3 causes a deterioration in the mechanical properties. In other words, the Al_4C_3 generated during the SPS process greatly affected the degradation of elongation due to its brittleness. That is why the elongation of 1vol% CNT reinforced composite was enhanced significantly compared to that of the 5vol% CNT reinforced composite, as indicated in Table 1.

We have discussed the effect of the formation of Al_4C_3 on the mechanical properties in the composite materials obtained. It is understood that some regions of the interfaces between the Al matrix and CNT in the SPSed compact and the extruded composite were combined by stable chemical bonding through the Al_4C_3 formed, as shown in Figure 11a and b. These structures were observed in our actual SPSed compact and the extruded composite (Fig. 4 and 6). It is believed that this chemically bonded structure is useful for stress transfer (Knocks, 2004; Kelly & Tyson, 1965; Lourie & Wagner, 1999; Fukuda & Chou, 1982) from the Al matrix to the CNT reinforcement. Moreover, the shape and position of the Al_4C_3 formed supported the enhancement of the mechanical properties. This is because the dumbbell shape of the Al_4C_3 which was formed on the tip of CNT can be held firmly and makes for an efficient stress transfer between the Al matrix and CNT, as shown in Figure 11c. The convex Al_4C_3 which is formed on the amorphous surface of the CNT not only functioned as a barrier to crack propagation due to the restraint of sliding, but also contributed to efficient stress transfer, as shown in Figure 11d. However, the existence of Al_4C_3 and well dispersed CNTs could also have interrupted the dislocation movements in the composites, resulting in the improvement in the mechanical properties of the composites (George et al., 2005; Oh et al., 2009; Jeong et al., 2007).

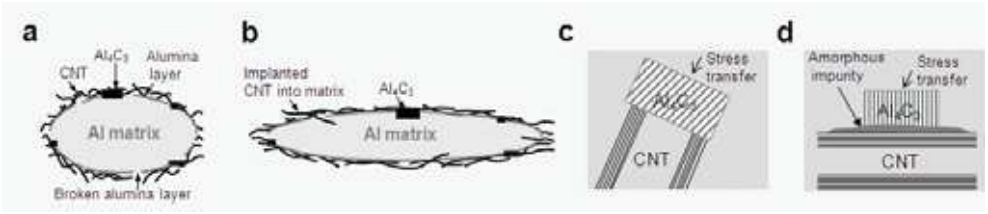

Fig. 11. Illustrations of structures of SPSed and extruded Al-CNT composites: (a) the generated Al_4C_3 and some parts of the broken alumina in the SPSed Al-CNT compact; (b) some of the CNT and Al_4C_3 implanted in the Al matrix in the extruded composites by mechanical pressure; (c) the dumbbell-shape and the convex-shape of Al_4C_3 which formed on the tip and surface of CNT and contributed to efficient stress transfer and a barrier to sliding.

Figure 12. shows the fracture surface of the Al-1and 5vol% CNT composites. Many dimples were observed in the Al matrix due to strong adhesion between particles. Several CNT bridges were observed near the cleavage regardless of the amount of CNT addition, as shown by the white arrow in Figure 12a and b. This CNT bridging also significantly contributed to the improvement in the mechanical properties. In particular, the 5vol% CNT composite showed a relatively large agglomeration of the CNTs compared to the 1vol% CNT composite (see black arrows in Fig. 12b and c). Moreover, several pointed-shape CNT

tips were observed in the fracture surface of the 1vol% CNT composite, which means that these CNTs were broken while extended, due to efficient stress transfer with strong chemical bonding created by Al_4C_3 between the Al matrix and CNT, as shown by the white arrows in Figure 12c. We also observed no shape change of the CNT tips in the fracture surface of 1vol% CNT composite. This indicated that this CNT did not include formation of Al_4C_3, which resulted in the pulling out of CNT being relatively easy, as shown by the black arrows in Figure 12c. Therefore, the Al_4C_3 generated during the SPS process is helpful in enhancing the Al-CNT composite materials. However, it must be accompanied by careful control in the quantity and size of Al_4C_3, which is brittle and hydrophilic (Ruch et al., 2006; Khalid et al., 2004).

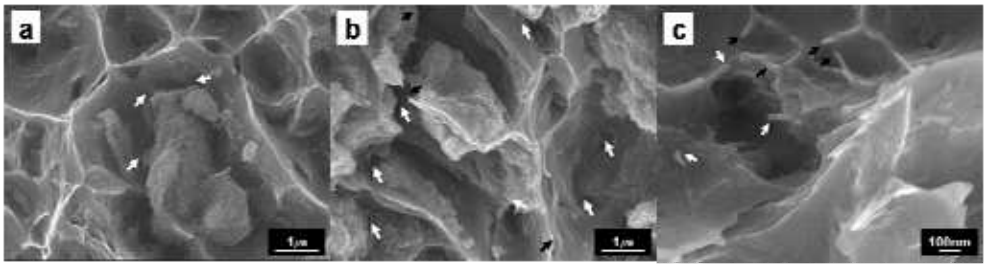

Fig. 12. FE-SEM micrographs of (a) the fracture surface of Al-1vol% CNT composite and (b) the Al-5vol% CNT composite after the tensile test; the white and black arrows indicate bridging and agglomeration of the CNTs. (c) High magnification of (a), where the white and black arrows indicate broken and pulled out CNT.

4. Conclusions

We have attempted to understand the effect of spark plasma sintering in fabricating Al-CNT composite materials which had highly enhanced tensile strength and no significant degradation of elongation compared to that of the pure Al bulk. Some parts of the Al oxide layer on the surface of the Al particles in the SPSed Al-CNT compact were broken during the SPS process, as confirmed by the DSC analysis and HR-TEM observation. Moreover, a small quantity of the Al_4C_3 was observed in the Al-CNT compact even though this was made under the solid state SPS temperature. The shape and formation position of Al_4C_3 also played an important role in the mechanical properties of the composites. The relative quantity of formed Al_4C_3 can be controlled by controlling the amount of CNT additions. We believe that the composites obtained were strengthened as a result of a complex phenomenon not only by the reinforcement of CNT but also through an efficient stress transfer effect by the chemical bonding between the Al matrix and CNT reinforcement through the Al_4C_3 formed during SPS process.

5. Acknowledgements

This research was partially supported by the New Energy and Industrial Technology Development Organization (NEDO) of Japan. We also would like to acknowledge Nissin Kogyo Co. Ltd for their technical support.

6. References

[1] Iijima, S. (1991). Helical microtubules of graphitic carbon. Nature, Vol. 354, pp. 56-58, ISSN 0028-0836.

[2] Endo, M.; Koyama, T. & Hishiyama, Y. (1976). Structural improvement of carbon fibers prepared from benzene. Jpn. J. Appl. Phys. Vol.15, pp. 2073-2076, ISSN 0021-4922.

[3] Niyogi, S.; Hamon, M. A.; Hu, H.; Zhao, B.; Bhowmik, P.; Sen, R.; Itkis, M. E. & Haddon, R. C. (2002). Chemistry of single-walled carbon nanotubes. Acc. Chem. Res. Vol. 35, pp. 1105-1113, ISSN 0001-4842.

[4] Komarov, F. F. & Mironov, A. M. (2004). Carbon nanotubes: presents and future. Phys. Chem. Solid State Vol. 5, pp. 411-429, ISSN 1729-4428.

[5] Salvetat-Delmotte, J. P. & Rubio, A. (2002). Mechanical properties of carbon nanotubes: a fiber digest for beginners. Carbon Vol. 40, pp. 1729-1734, ISSN 0008-6223.

[6] Hilding, J.; Grulke, E. A.; Zhang, Z. G. & Lockwood, F. (2003). Dispersion of Carbon Nanotubes in Liquids. J. Dispersion Sci. Tech. Vol. 24, pp. 1-41, ISSN 0193-2691.

[7] Xu, C. L.; Wie, B. Q.; Ma, R. Z.; Liang, J.; Ma, X. K. & Wu D. H. (1999) Fabrication of aluminum–carbon nanotube composites and their electrical properties. Carbon Vol. 37, pp. 855-858, ISSN 0008-6223.

[8] Kuzumaki, T.; Hayashi, T.; Miyazawa, K.; Ichinose, H.; Ito, K. & Ishida, Y. (1998). Processing of ductile carbon nanotube/C60 composite. Mater. Trans. Vol. 38, pp. 574-577, ISSN 1347-5320.

[9] Kuzumaki, T.; Miyazawa, K.; Ichinose, H. & Ito, K. (1998). Processing of carbon nanotube reinforced aluminum composite. J. Mater. Res. Vol. 9, pp. 2445-2449, ISSN 0884-2914.

[10] Sridhar, I. & Narayana, K. R. (2009). Processing and characterizations of MWCNT reinforced aluminum matrix composites. J. Mater. Sci. Vol. 44, pp. 1750-1756, ISSN 1573-4803.

[11] Deng, C. F.; Zhang, X. X.; Wang, D.; Lin, Q. & Li, A. (2007). Preparation and characterization of carvon nanotuves/aluminum matris composites. Mater. Lett. Vol. 61, pp. 1725-1728, ISSN 0167-577X.

[12] Bakshi, S. R.; Keshri, A. K.; Singh, V.; Seal, S. & Agarwal, A. (2009). Interface in carbon nanotube reinforced aluminum silicon composites: thermodynamic analysis and experimental verification. J. Alloys Compd. Vol. 481, pp. 207-213, ISSN 0925-8388.

[13] Lahiri, D.; Bakshi, S. R.; Keshri, A. K.; Liu, Y. & Agarwa, A. (2009). Dual strengthening mechanisms induced by carbon nanotubes in roll bonded aluminum composites. Mater. Sci. Eng. A Vol. 523, pp. 263-270, ISSN 0921-5093.

[14] Deng, C.; Zhang, X.; Ma, Y. & Wang, D. (2007). Fabrication of aluminum matrix composite reinforced with carbon nanotubes. Rare Metals Vol. 26, pp. 450-455, ISSN 1001-0521.

[15] Deng, C.; Wang, D.; Zhang, X. & Li, A. (2007). Processing and properties of carbon nanotubes reinforced aluminum composites. Mater. Sci. Eng. A Vol. 444, pp. 138-145, ISSN 0921-5093.

[16] Esawi, A. M. K.; & Morsi, K. (2007). Dispersion of carbon nanotubes (CNT) in aluminium powder. Composites Part A Vol. 3, pp. 646-650, ISSN 1359-835X.

[17] Esawi, A. M. K. & Borady, M. (2008). Carbon nanotube-reinforced aluminum strips. Compos. Sci. Technol. Vol. 68, pp. 486-492, ISSN 0266-3538.

[18] Esawi, A. M. K.; Morsi, K.; Sayed, A.; Gawad, A. A. & Borah, P. (2009). Fabrication and properties of dispersed carbon nanotube - aluminum composites. Mater. Sci. Eng. A Vol. 508, pp. 167-173, ISSN 0921-5093.

[19] Morsi, K; El-Desouky, A.; Johnson, B.; Mar, A. & Lanka, S. (2009). Spark plasma extrusion (SPE): Prospects and potential. Scr. Mater. Vol. 61, pp. 395-398, ISSN 1359-6462.

[20] Morsi, K.; Esawi, A. M. K.; Lanka, S.; Sayed, A. & Taher, M. (2010). Spark plasma extrusion (SPE) of ball-milled aluminumand carbon nanotube reinforced aluminum composite powders. Composites: Part A Vol. 41, pp. 322-326, ISSN ISSN 1359-835X.

[21] Laha, T.; Agarwal, A.; Mckechnie, T. & Seal, S. (2004). Synthesis and characterization of plasma spray formed carbon nanotube reinforced aluminum composite. Mater. Sci. Eng. A Vol. 381, pp. 249-258, ISSN ISSN 0921-5093.

[22] Bakshi, S. R.; Singh, V.; Balani, K.; Mccartney, D. G.; Seal, S. & Agarwal, A. (2008). Carbon nanotube reinforced aluminum composite coating via cold spraying. Surf. Coat. Technol. Vol. 202, pp. 5162-5169, ISSN 0257-8972.

[23] Bakshi, S. R.; Lahiri, D. & Agarwal, A. (2010). Carbon nanotube reinforced metal matrix composites -a review. Inter. Mater. Rev. Vol. 55, pp. 41-64, ISSN 1743-2804.

[24] Kwon, H.; Estili, M.; Takagi, K.; Miyazaki, T. & Kawasaki, A. (2009). Combination of hot extrusion and spark plasma sintering for producing carbon nanotube reinforced aluminum matrix composites. Carbon Vol. 47, pp. 570-577, ISSN 0008-6223.

[25] Kwon, H. & Kawasaki, A. (2009). Extrusion of spark plasma sintered aluminum-carbon nanotube composites at various sintering temperatures. J. Nanosci. Nanotechno Vol. l 9, pp. 6542-6548, ISSN 1550-7033.

[26] Kwon, H.; Park, D.; Silvain, J. F. & Kawasaki, A. (2010). Investigation of carbon nanotube reinforced aluminum matrix composite materials. Compos. Sci. Technol. Vol. 70, pp. 546-550, ISSN 0266-3538.

[27] Noguchi, T.; Magario, A.; Fukazawa, S.; Shimizu, S.; Beppu, J. & Seki, M. (2004). Carbon Nanotube/Aluminium Composites with Uniform Dispersion. Mater. Trans. Vol. 45, pp. 602-604, ISSN 1347-5320.

[28] Keszler, A. M.; Nemes, L.; Ahmad, S. R. & Fang, X. (2004). Characterisation of carbon nanotube materials by Raman spectroscopy and microscopy - A case study of multiwalled and singlewalled samples. J. Optoelectron. Adv. Mater. Vol. 6, pp. 1269-1274, ISSN 1454-4164.

[29] Zhao, Q. & Wagner, H. D. (2004). Raman spectroscopy of carbon-nanotube-based composites. Philos. Trans. R. Soc. Vol. 362, pp. 2407-2424, ISSN 1471-2962.

[30] http://en.wikipedia.org/wiki/Tensile_strength

[31] Kocks U. F. (2004). Solution hardening and strain hardening at elevated temperatures. American Society for Metal. Metals Park, OH, pp. 89-107.

[32] Kelly, A. & Tyson, W. R. (1965). Tensile properties of fibre-reinforced metals: Copper/tungsten and copper/molybdenum. J. Mech. Phys. Solids Vol. 13, pp. 329-338, ISSN 0022-5096.

[33] Cox, H. L. (1952). The elasticity and strength of paper and other fibrous materials. Br. J. Appl. Phys. Vol. 3, pp. 72-79, ISSN 0508-3443.

[34] Serajzadeh, S. (2004). Prediction of dynamic recrystallization kinetics during hot rolling. Modelling Simul. Mater. Sci. Eng. Vol. 12, pp. 1185-1200, ISSN 1361-651X.

[35] Zadra, M.; Casari, F.; Girardini, L. & Molinari, A. (2007). Spark plasma sintering of pure aluminium powder: mechanical properties and fracture analysis. Powder Metall. Vol. 50, pp. 40-45, ISSN 1743-2901.

[36] Omori, M. (2000). Sintering, consolidation, reaction and crystal growth by the spark plasma system (SPS). Mater. Sci. Eng. A Vol. 287, pp. 183-188, ISSN 0921-5093.

[37] Xie, G.; Ohashi, O.; Yoshioka, T.; Song, M.; Mitsuishi, K.; Yasuda, H.; Furuya, K. & Noda, T. (2001). Effect of Interface Behavior between Particles on Properties of Pure Al Powder Compacts by Spark Plasma Sintering. Mater. Trans. Vol. 42, pp. 1846-1849, ISSN 1347-5320.

[38] Kwon, H.; Park, D.; Park, Y.; Silvain, J. F.; Kawasaki, A. & Park, Y. (2010). Spark plasma sintering behavior of pure aluminum depending on various sintering temperatures. Met. Mater. Int. Vol. 16, pp. 71-75, ISSN 1598-9623.

[39] Ci, L.; Ryu, Z.; Jin-Phillipp, N. Y. & Rühle, M. (2006). Investigation of the interfacial reaction between multi-walled carbon nanotubes and aluminum. Acta Mater. Vol. 54, pp. 5367-5375, ISSN 1359-6454.

[40] Laha, T. & Agarwal, A. (2008). Effect of sintering on thermally sprayed carbon nanotube reinforced aluminum nanocomposite. Mater. Sci. Eng. A Vol. 480, pp. 323-332, ISSN 0921-5093.

[41] Laha, T.; Kuchibhatla, S.; Seal, S.; Li, W. & Agarwal, A. (2007) Interfacial phenomena in thermally sprayed multiwalled carbon nanotube reinforced aluminum nanocomposite. Acta Mater. Vol. 55, pp. 1059-1066, ISSN 1359-6454.

[42] Nagae, T.; Tomiya, S. & Yokota, N. (2001). Compaction and application of the aluminum powder by spark plasma sintering process. Toyama Industrial Technology Center *Vol.* 89, pp. 89-93 (In Japanese), ISSN 0914-2207

[43] Lourie, O. & Wagner, H. D. (1999). Evidence of stress transfer and formation of fracture clusters in carbon nanotube-based composites. Compos. Sci. Technol. Vol. 59, pp. 975-977, ISSN 0266-3538.

[44] Fukuda, H. & Chou, T. W. (1982). A probabilistic theory of the strength of short-fibre composites with variable fibre length and orientation. J. Mater. Sci. Vol. 17, pp. 1003-1011, ISSN 1573-4803.

[45] George, R.; Kashyap, K. T.; Rahul, R. & Yamadagni S. (2005). Strengthening in carbon nanotube/aluminium (CNT/Al) composites.Scr. Mater. Vol. 53, pp. 1159-1163, ISSN 1359-6462.

[46] Oh, S. H.; Legros, M.; Kiener, D. & Dehm, D. (2009). In situ observation of dislocation nucleation and escape in a submicrometre aluminium single crystal. Nature Mater. Vol. 8, pp. 95-100, ISSN 1476-1122.

[47] Jeong, Y. J.; Cha, S. I.; Kim, K. T.; Lee, K. H.; Mo, C. B. & Hong, S. H. (2007). Synergistic Strengthening Effect of Ultrafine-Grained Metals Reinforced with Carbon Nanotubes. Small Vol. 5, pp. 840-844, ISSN 1613-6829.

[48] Ruch, P. W.; Beffort, O.; Kleiner, S.; Weber, L. & Uggowitzer, P. J. (2006). Slective interfacial bonding in Al(Si)-diamond composites and its effect on thermal conduvtivity. Compos. Sci. Technol. Vol. 66, pp. 2677-2685, ISSN 0266-3538.

[49] Khalid, F. A.; Beffort, O.; Klotz, U. E.; Keller, B. A. & Gasser, P. (2004). Microstructure and interfacial characteristics of aluminum-diamond composite materials. Diamond Relat. Mater. Vol. 13, pp. 393-400, ISSN 0925-9635.

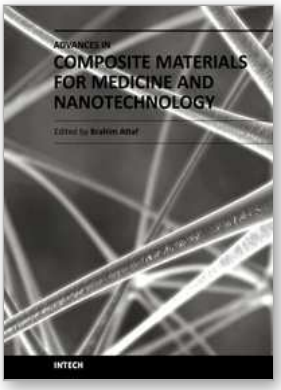

Advances in Composite Materials for Medicine and Nanotechnology

Edited by Dr. Brahim Attaf

ISBN 978-953-307-235-7
Hard cover, 648 pages
Publisher InTech
Published online 01, April, 2011
Published in print edition April, 2011

Due to their good mechanical characteristics in terms of stiffness and strength coupled with mass-saving advantage and other attractive physico-chemical properties, composite materials are successfully used in medicine and nanotechnology fields. To this end, the chapters composing the book have been divided into the following sections: medicine, dental and pharmaceutical applications; nanocomposites for energy efficiency; characterization and fabrication, all of which provide an invaluable overview of this fascinating subject area. The book presents, in addition, some studies carried out in orthopedic and stomatological applications and others aiming to design and produce new devices using the latest advances in nanotechnology. This wide variety of theoretical, numerical and experimental results can help specialists involved in these disciplines to enhance competitiveness and innovation.

InTech Europe
University Campus STeP Ri
Slavka Krautzeka 83/A
51000 Rijeka, Croatia
Phone: +385 (51) 770 447
Fax: +385 (51) 686 166
www.intechopen.com

InTech China
Unit 405, Office Block, Hotel Equatorial Shanghai
No.65, Yan An Road (West), Shanghai, 200040, China
中国上海市延安西路65号上海国际贵都大饭店办公楼405单元
Phone: +86-21-62489820
Fax: +86-21-62489821